Letter Vol. 48, No. 2 / 15 January 2023 / *Optics Letters* 239

Optics Letters

# High-efficiency mid-infrared on-chip silicon grating couplers for perfectly vertical coupling

**YUHENG LIU,[1] LIPENG XIA,[1] TING LI,[1] YUHAN SUN,[1] PEIJI ZHOU,[1] LI SHEN,[2,4] AND YI ZOU[1,3,*]**

[1] *The School of Information Science and Technology, ShanghaiTech University, Shanghai, 201210, China*
[2] *Wuhan National Laboratory for Optoelectronics and School of Optical and Electronic Information, Huazhong University of Science and Technology, Wuhan, Hubei 430074, China*
[3] *Shanghai Engineering Research Center of Energy Efficient and Custom AI IC, Shanghai 201210, China*
[4] *lishen@hust.edu.cn*
**zouyi@shanghaitech.edu.cn*

*Received 18 October 2022; revised 29 November 2022; accepted 7 December 2022; posted 8 December 2022; published 2 January 2023*

**We present, to our knowledge, the first experimental demonstration of two on-chip gratings for perfectly vertical coupling at wavelengths of 3350 nm and 3550 nm, respectively. An anti-backreflection unit containing a fully etched trench and a subwavelength pillar is introduced in each grating period, together with a binary-approximated blazed unit, interleaving fully and shallow-etched slots in 500-nm thick silicon film. Both gratings show a strong ability to eliminate backreflection and provide predicted directionality of around 80%. The physical theoretical analysis is applied during further apodization for mitigating the computation of the optimization algorithm, improving the efficiency and optimization reliability, and increasing the fabrication robustness. The measured coupling efficiencies (CEs) of the gratings are −5.58 dB and −4.34 dB at wavelengths of 3350 nm and 3550 nm, with a 3-dB bandwidth of at least 87 nm and 210 nm, respectively.**

https://doi.org/10.1364/OL.478751

The mid-infrared (MIR) region (2–20 μm) is attractive since it covers two atmospheric transparency windows (3–5 μm and 8–12 μm) that contain the strong characteristic vibrational transitions of many important molecules [1]. It is essential for free-space optical communication, thermal imaging, industry safety monitoring, and environmental gas detection. On-chip MIR devices are based on various types of photonics platform [1], such as silicon-on-insulator (SOI), silicon-on-sapphire (SOS), and germanium-on-silicon (GOS). Of these, SOI is one of the most preferred platforms, owing to its low cost, high refractive index contrast, and CMOS compatibility [1]. Most devices on SOI without undercutting operate below 3.6 μm, which is useful for sensing some volatile organic compounds, such as HCl and $CH_4$ [2,3]. By adopting special designs [4,5], this wavelength limit, which is from the strong absorption of the buried box layer [6,7], could be surmountable. This extends the operating bandwidth to cover the first atmospheric transparency window of 3–5 μm.

Photonic integrated devices, e.g., silicon or germanium devices, usually require optical fibers to deliver external light sources into chips. However, highly efficient coupling is challenging, owing to the huge mode mismatch between on-chip waveguides and optical fibers. As a result, developing high-efficiency coupling methods between optical fibers and chips is essential. Of the common coupling techniques [8], grating couplings are often preferred because of their simpler fabrication process and larger fiber alignment tolerance. This also allows in situ wafer-scale testing without additional steps.

Figure 1 summarizes recent advances in MIR grating couplers [9–20]. Most of them are in the wavelength range of 2–2.75 μm, while the wavelength range of 3–5 μm, which is the atmospheric window, is underexplored. In particular, there is no report about perfectly vertical coupling in MIR, which has gained more attraction than tilted gratings for its easy alignment and packaging and as a potential solution for realizing high-density coupling [21].

In this Letter, we demonstrate two high-efficiency grating couplers on SOI for perfectly vertical coupling. The measured coupling efficiencies (CEs) are −5.58 dB and −4.34 dB for TE polarization at wavelengths of 3350 nm and 3550 nm, respectively. The corresponding 3-dB bandwidths are >87 nm and 210 nm, respectively. This is, to our knowledge, the first experimental demonstration of perfectly vertical gratings on SOI for the MIR. It fills the gap of SOI-based grating couplers at the wavelength range from 3.3 to 3.6 μm and improves the coupling efficiency and bandwidth, as shown in Fig. 1.

Figure 2 illustrates the proposed grating coupler, consisting of a subwavelength anti-backreflection (ABR) unit and a binary-approximated blazed (BAB) structure in each period. Specifically, the ABR unit contains a fully etched slot and an unetched silicon pillar, whose widths are denoted $e_1$ and $w_1$, respectively. Blazed structures have been reported to provide great coupling directionality [8,22,23], which is defined as the ratio of the power transmitted toward fibers to the total power in other directions. We use a BAB structure, specifically, an L shape, to ease the fabrication. The BAB unit contains a fully etched slot, a shallow-etched pillar, and an unetched pillar, whose

0146-9592/23/020239-04 Journal © 2023 Optica Publishing Group

Corrected 10 January 2023

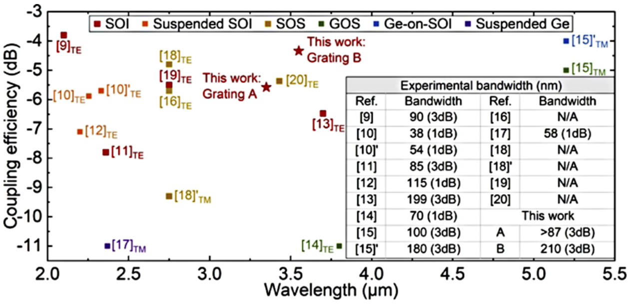

| Experimental bandwidth (nm) | | | |
|---|---|---|---|
| Ref. | Bandwidth | Ref. | Bandwidth |
| [9] | 90 (3dB) | [16] | N/A |
| [10] | 38 (1dB) | [17] | 58 (1dB) |
| [10]' | 54 (1dB) | [18] | N/A |
| [11] | 85 (3dB) | [18]' | N/A |
| [12] | 115 (1dB) | [19] | N/A |
| [13] | 199 (3dB) | [20] | N/A |
| [14] | 70 (1dB) | This work | |
| [15] | 100 (3dB) | A | >87 (3dB) |
| [15]' | 180 (3dB) | B | 210 (3dB) |

**Fig. 1.** Summary of advances in MIR grating couplers.

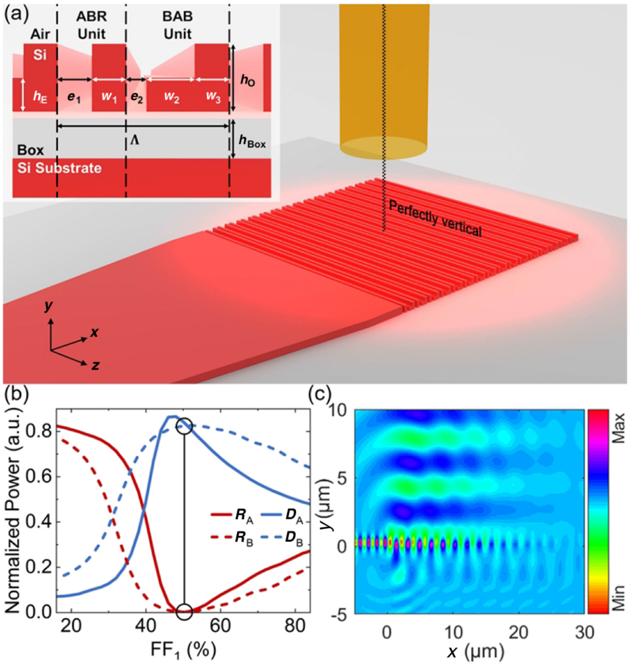

**Fig. 2.** (a) Schematic and (inset) structure parameters of proposed grating coupler. (b) Variations of backreflection ($R$) and directionality ($D$) as a function of $\text{FF}_1$ of Grating A (3350 nm) and Grating B (3550 nm). (c) Simulated electric field profile of Grating B.

widths are denoted $e_2$, $w_2$, and $w_3$, respectively. The total width of each grating period is Λ, while the thicknesses of the SOI silicon film $h_O$ and the box layer $h_{Box}$ are 500 nm and 3 μm, respectively. The height of the shallow-etched structure is $h_E$. We denote the filling factor (FF) of the ABR unit's width $e_1 + w_1$ to the local period's width Λ as $\text{FF}_0$., while $\text{FF}_1$ represents the ratio of $e_1$ to the entire ABR unit's width, $e_1 + w_1$. In addition, $\text{FF}_2$ and $\text{FF}_3$ denote the ratio of $e_2$ to the entire BAB unit's width, $e_2 + w_2 + w_3$ and the ratio of $w_2$ to the L-shaped structure width, $w_2 + w_3$.

Preliminary designs are carried out using a commercially available finite-difference time-domain (FDTD) solution. We write a customized particle swarm optimization (PSO) program to solve the parameters, i.e., Λ, $\text{FF}_0$, $\text{FF}_1$, $\text{FF}_2$, $\text{FF}_3$, and $h_E$. As preliminary results, for grating couplers with uniform periods, the thickness of the shallow-etched parts $h_E$ is 230 nm, and other parameters are given in Table 1.

To better illustrate the role of the ABR and the BAB units, we plot the backreflection ($R$) and the directionality ($D$) as a function of $\text{FF}_1$ in Fig. 2. For uniform gratings with optimized parameters [circles in Fig. 2(b)], the equivalent refractive indices of both the ABR and BAB units are nearly equal, resulting in negligible backreflection. Changing $\text{FF}_1$ may affect the smooth transition of refractive indices of different units, which leads to a significant increase of the backreflection. Moreover, the variation trends of backreflection and directionality are opposite. This has the consequence that the remaining light, which can be regarded as the directionality here, since the power transmitting toward the substrate or directly through the grating region is very low, is dominated by the unchanged blazed units.

**Table 1. Preliminary Structure Parameters for Couplers with Uniform Periods**

| | Λ / μm | $\text{FF}_0$ | $\text{FF}_1$ | $\text{FF}_2$ | $\text{FF}_3$ |
|---|---|---|---|---|---|
| Grating A (3350 nm) | 1.52 | 0.24 | 0.5 | 0.22 | 0.56 |
| Grating B (3550 nm) | 1.6 | 0.26 | 0.52 | 0.22 | 0.74 |

Although the preliminary designs for both gratings have a directionality of around 80%, the overlaps between the diffracted light fields and the fundamental fiber mode are low, which decreases the overall CEs. We thus design optimization using a customized PSO algorithm to mitigate the mismatched issue. Considering the chalcogenide MIR fiber (IRF-S-7) that we used, we set the refractive index of the fiber to 2.4 and the numerical aperture (NA) to 0.3. The sizes of the couplers are fixed at 30 × 30 μm to match the large NA of the fiber, and the thickness of the shallow-etched structures, $h_E$, remains the same. Here, unlike the typical approach that modifies the FF of a grating while keeping the period, we chirp the grating periods Λ when apodizing them. After fixing the values of $h_E$ and Λ, the remaining four of the six grating parameters, which are $\text{FF}_0$, $\text{FF}_1$, $\text{FF}_2$, and $\text{FF}_3$, are decided using the following method.

In traditional apodization, the FF $F$, defined as the ratio of the unetched section to the local period, can be expressed as [24]

$$F = F_0 - R \times z, \tag{1}$$

where $F_0$ is the FF of the first grating period, $R$ is a linear apodization coefficient, and $z$ is the distance from the starting point of the grating to each period. As illustrated previously, since the BAB units dominate the diffracted mode profile, we would apply Eq. (1) to the BAB units only, and adjust $\text{FF}_1$ of the ABR units to ensure similar equivalent refractive indices. Thus, the ratio of the width of the BAB structure to the entire blazed unit, which is $1 - \text{FF}_2$, becomes $F$ in Eq. (1) for the following optimization. In other words, $1 - \text{F}_0$ is equal to the value of the $\text{FF}_2$ in the periodic design, shown in Table 1. Moreover, $R$ is a variable to be solved by PSO, and $z$ is decided by each grating period Λ, which can be solved by using

$$\Lambda = \frac{\lambda}{n_{\text{eff\_blazed}}}, \tag{2}$$

where $\lambda$ is the working wavelength of the grating, and $n_{\text{eff\_blazed}}$ is the effective refractive index of the blazed unit in each period. Note that since we are interested in designing a perfectly vertical grating coupler, we set the diffraction angle to zero. To acquire $n_{\text{eff\_blazed}}$, we first determine the effective refractive indices of the three sections in the BAB unit, i.e., the fully etched section, the shallow-etched section, and the unetched pillar, by applying the dispersion equation for TE modes [25,26]:

$$\sqrt{n_\mathrm{f}^2 - N_\mathrm{eff}^2} \times \frac{2\pi}{\lambda} h = m\pi + \tan^{-1}\sqrt{\frac{N_\mathrm{eff}^2 - n_\mathrm{c}^2}{n_\mathrm{f}^2 - N_\mathrm{eff}^2}} + \tan^{-1}\sqrt{\frac{N_\mathrm{eff}^2 - n_\mathrm{s}^2}{n_\mathrm{f}^2 - N_\mathrm{eff}^2}} \quad (m = 0, \pm 1, \pm 2, \ldots), \tag{3}$$

where $n_\mathrm{c}$ and $n_\mathrm{s}$ are the refractive indices of the cladding and substrate media, respectively, $N_\mathrm{eff}$ is the effective index, and $h$ is the thickness of structures.

Then, by applying Eq. (4) twice, we can derive $n_\mathrm{eff\_blazed}$:

$$n_\mathrm{eff} = \sqrt{f \times N_{\mathrm{eff}_1}^2 + (1 - f) \times N_{\mathrm{eff}_2}^2}, \tag{4}$$

where $f$ is the FF and $N_\mathrm{eff\_1}$ and $N_\mathrm{eff\_2}$ are the two different effective indices. When calculating the effective index of the L-shaped structure, we replace $f$ with the $\mathrm{FF}_3$ predicted by the PSO, and substitute $N_\mathrm{eff\_1}$ and $N_\mathrm{eff\_2}$ with $N_\mathrm{eff\_E}$ and $N_\mathrm{eff\_O}$, respectively. Here, $N_\mathrm{eff\_E}$ and $N_\mathrm{eff\_O}$ represent the effective indices of the shallow-etched and the unetched sections. Finally, since a BAB unit consists of a fully etched slot and an L-shaped structure, by replacing $f$, $N_\mathrm{eff\_1}$, and $N_\mathrm{eff\_2}$ with $\mathrm{FF}_2$, $n_\mathrm{air} = 1$, and the index just derived, we can solve for $n_\mathrm{eff\_blazed}$. Substituting these parameters, we convert Eq. (2) into

$$\Lambda = \frac{\lambda}{\sqrt{FF_2 + (1 - FF_2)[FF_3 \times N_{\mathrm{eff_E}}^2 + (1 - FF_3) \times N_{\mathrm{eff_O}}^2]}}. \tag{5}$$

Consequently, the five parameters of each grating period are considered in the optimization; these are Λ, $\mathrm{FF}_0$, $\mathrm{FF}_1$, $\mathrm{FF}_2$, and $\mathrm{FF}_3$. A group of varied $\mathrm{FF}_3$ is first predicted by the PSO. Next, the Λ in the first period is solved using Eq. (5) by applying the initial value of $\mathrm{FF}_2$ given in Table 1. Then the values of $\mathrm{FF}_2$ and Λ in the following periods are solved one by one by substituting each other into Eq. (1) and Eq. (5). The values of $\mathrm{FF}_1$ and $\mathrm{FF}_0$ are determined by PSO to cope with the change of the equivalent refractive indices in the BAB sections.

Since one of the parameters is determined from physical principles, the computation effort of the optimization algorithm is greatly reduced. Thus, the cost of taking all coefficients into consideration at the same time becomes affordable. This ensures the reliability of the optimization results. It avoids the situation that only some of the parameters are calculated at a time, owing to too many parameters and too much computation, which will often fail to obtain the global optimal solution. The optimized overlaps between the diffracted field and the fiber mode are 84% and 82% for 3350 nm and 3550 nm gratings, respectively, leading to simulated CEs of about −1.68 dB and −1.78 dB at wavelengths of 3350 nm and 3550 nm, respectively. Figure 2(c) displays the simulated optical field profile of the 3550 nm grating; we observe a perfectly vertical output field. The optimized grating parameters and the simulated CEs are shown in Figs. 3 and 4, respectively. As shown in Fig. 3, the backreflection at the center wavelengths of both gratings is about −30 dB.

Figure 4 displays a scanning electron micrograph of the fabricated grating coupler and the measurement setup, where the CE is measured through two grating couplers connected with a tapered straight waveguide. The devices were fabricated in ShanghaiTech University Quantum Device Lab. The detailed fabrication process is given by Zhang *et al.* [27]. During the measurement, collimated linearly polarized light emitted from a tunable quantum cascade laser is first coupled into an input chalcogenide MIR fiber (IRF-S-7) using a reflective collimator. The polarization status after passing the 1-m-long chalcogenide fiber is characterized for later coupling efficiency calculation. The light is then coupled into the chip through the proposed

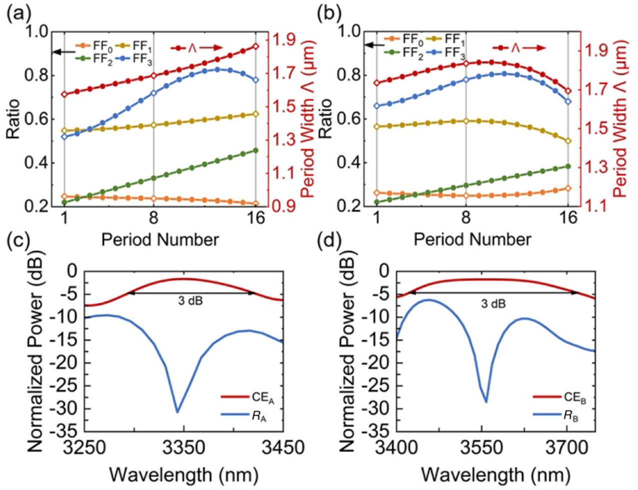

**Fig. 3.** (a, b) Optimized parameters of apodized (a) Grating A (3350 nm) and (b) Grating B (3550 nm). Solid symbols represent the value of each parameter and hollow symbols are sample points used in the PSO, which finally decides the polynomial variation of parameter curves. There are no hollow symbols on the curve of $\mathrm{FF}_2$, since it is completely derived by Eq. (1). (c, d) Simulated CE and $R$ of apodized (c) Grating A (3350 nm) and (d) Grating B (3550 nm).

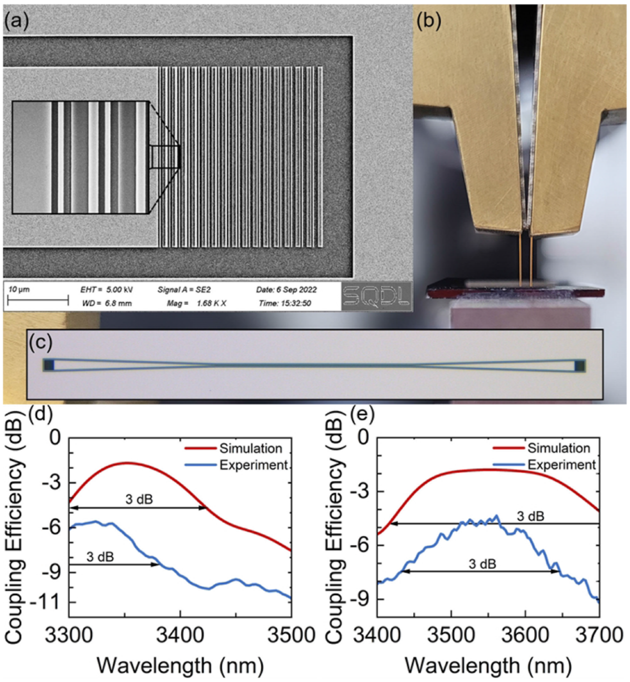

**Fig. 4.** (a) Scanning electron micrograph of fabricated grating coupler. Inset: enlargement of grating coupler. (b) Measurement setup. (c) Optical micrograph of testing device. (d, e) Simulated and measured results of (d) Grating A (3350 nm) and (e) Grating B (3550 nm).

grating coupler. The output signal from the output grating coupler is collected by a chalcogenide MIR fiber and sent to an optical spectrum analyzer (YOKOGAWA AQ6377). The experimental results are plotted in Fig. 4, of which we assume that the losses of both input and output gratings are equal and the propagation loss is negligible. Compared with the simulated CE of −1.68 dB at the fundamental mode of an IRF-S-7 fiber, with a 3-dB bandwidth of around 130 nm at a wavelength of 3350 nm, the measured efficiency peak is about −5.58 dB at 3324 nm, with a bandwidth of at least 87 nm, which is limited by the shortest available wavelength (3300 nm) of the laser used in the experiment. The simulated CE of the 3550 nm grating is about −1.78 dB and the 3-dB bandwidth is around 300 nm. The experimental result is −4.34 dB at 3561 nm with a 3-dB bandwidth of ≈210 nm. The limitation to achieving higher coupling efficiency is mainly from the approximated blazed structure, which decreases its ability to concentrate the diffraction into a single order. The small number of sampling points during the optimization, to reduce computation, also affects the couplers' performances. The shift of the peak wavelength and the decrease in the measured CEs mainly come from the fabrication process. During fabrication, the alignment error between two exposures for shallow-etched and fully etched structures can reach up to 40 nm, which is roughly 20% of the width of the ABR sections. Other fabrication errors, such as over-etching at structure edges and an incorrect etch depth, also affect the CE and the peak wavelength. In addition, the size of the mode field of the fibers is relatively sensitive to the distance between the chip and the fiber facet, owing to the large NA of the chalcogenide fibers we used, which may lead to different fiber conditions between the simulation and experiment.

In conclusion, we report the first demonstration of high-efficiency grating couplers for perfect vertical coupling in MIR. By exploiting ABR units and blazed structures, together with an apodization process, we experimentally achieve CEs of −5.58 dB and −4.34 dB with a 3-dB bandwidth of at least 87 nm and 210 nm for the two target wavelengths of 3350 nm and 3550 nm, respectively. The performance can be further improved by either improving fabrication procedures or increasing the undetermined parameters considered in the optimization. For example, by utilizing a gray-scale patterning approach, it is possible to develop a perfectly shaped blazed grating coupler with higher perfectly vertical coupling efficiency. We believe that the demonstrated perfectly vertical couplers have the potential to further advance the development of MIR couplers. They can also facilitate optical MIR applications, such as multicore-fiber-based space division multiplexing, and thus lay the foundation for highly integrated MIR optical applications in the future.

**Funding.** Natural Science Foundation of Shanghai (21ZR1443100); National Natural Science Foundation of China (61705099, 62175080).

**Acknowledgments.** We thank the ShanghaiTech University Quantum Device Lab (SQDL) for technical support.

**Disclosures.** The authors declare no conflicts of interest.

**Data availability.** Data underlying the results presented in this paper are not publicly available at this time but may be obtained from the authors upon reasonable request.

## REFERENCES

1. Y. Zou, S. Chakravarty, C.-J. Chung, X. Xu, and R. T. Chen, Photonics Res. **6**, 254 (2018).
2. J. Hodgkinson and R. P. Tatam, Meas. Sci. Technol. **24**, 012004 (2013).
3. A. Schliesser, N. Picqué, and T. W. Hänsch, Nat. Photonics **6**, 440 (2012).
4. P. T. Lin, V. Singh, J. Hu, K. Richardson, J. D. Musgraves, I. Luzinov, J. Hensley, L. C. Kimerling, and A. Agarwal, Lab Chip **13**, 2161 (2013).
5. F. Ottonello-Briano, C. Errando-Herranz, H. Rödjegård, H. Martin, H. Sohlström, and K. B. Gylfason, Opt. Lett. **45**, 109 (2020).
6. R. Soref, Nat. Photonics **4**, 495 (2010).
7. S. A. Miller, M. Yu, X. Ji, A. G. Griffith, J. Cardenas, A. L. Gaeta, and M. Lipson, Optica **4**, 707 (2017).
8. R. Marchetti, C. Lacava, L. Carroll, K. Gradkowski, and P. Minzioni, Photonics Res. **7**, 201 (2019).
9. N. Hattasan, B. Kuyken, F. Leo, E. M. P. Ryckeboer, D. Vermeulen, and G. Roelkens, IEEE Photonics Technol. Lett. **24**, 1536 (2012).
10. W. Zhou and H. K. Tsang, Opt. Lett. **44**, 3621 (2019).
11. W. Chen, J. Wu, D. Wan, J. Wang, J. Wang, Y. Zou, Z. Cheng, and T. Liu, J. Phys. D: Appl. Phys. **55**, 015109 (2022).
12. R. Guo, H. Gao, T. Liu, and Z. Cheng, Opt. Lett. **47**, 1226 (2022).
13. N. Chen, B. Dong, X. Luo, H. Wang, N. Singh, G.-Q. Lo, and C. Lee, Opt. Express **26**, 26242 (2018).
14. C. Alonso-Ramos, M. Nedeljkovic, D. Benedikovic, J. S. Penadés, C. G. Littlejohns, A. Z. Khokhar, D. Pérez-Galacho, L. Vivien, P. Cheben, and G. Z. Mashanovich, Opt. Lett. **41**, 4324 (2016).
15. S. Radosavljevic, B. Kuyken, and G. Roelkens, Opt. Express **25**, 19034 (2017).
16. X. Chen, C. Li, and H. K. Tsang, in *2009 14th OptoElectronics and Communications Conference*, (IEEE, 2009), pp. 1–2.
17. J. Kang, Z. Cheng, W. Zhou, T.-H. Xiao, K.-L. Gopalakrisna, M. Takenaka, H. K. Tsang, and K. Goda, Opt. Lett. **42**, 2094 (2017).
18. Z. Cheng, X. Chen, C. Y. Wong, K. Xu, C. K. Y. Fung, Y. M. Chen, and H. K. Tsang, IEEE Photonics J. **4**, 104 (2012).
19. Z. Cheng, X. Chen, C. Yan Wong, K. Xu, and H. Ki Tsang, Opt. Lett. **37**, 5181 (2012).
20. Y. Zou, H. Subbaraman, S. Chakravarty, X. Xu, A. Hosseini, W.-C. Lai, P. Wray, and R. T. Chen, Opt. Lett. **39**, 3070 (2014).
21. T. Watanabe, M. Ayata, U. Koch, Y. Fedoryshyn, and J. Leuthold, J. Lightwave Technol. **35**, 4663 (2017).
22. C. Alonso-Ramos, P. Cheben, A. Ortega-Moñux, J. H. Schmid, D. X. Xu, and I. Molina-Fernández, Opt. Lett. **39**, 5351 (2014).
23. D. Benedikovic, C. Alonso-Ramos, S. Guerber, X. Le Roux, P. Cheben, C. Dupré, B. Szelag, D. Fowler, É Cassan, D. Marris-Morini, C. Baudot, F. Boeuf, and L. Vivien, Opt. Express **27**, 26239 (2019).
24. R. Marchetti, C. Lacava, A. Khokhar, X. Chen, I. Cristiani, D. J. Richardson, G. T. Reed, P. Petropoulos, and P. Minzioni, Sci. Rep. **7**, 16670 (2017).
25. J. Yang, Z. Zhou, H. Jia, X. Zhang, and S. Qin, Opt. Lett. **36**, 2614 (2011).
26. J. Xu, S. Yang, L. Wu, L. Xu, Y. Li, R. Liao, M. Qu, X. Quan, and X. Cheng, Opt. Express **29**, 42999 (2021).
27. A. Zhang, L. Xia, T. Li, C. Chang, P. Zhou, X. Xu, and Y. Zou, Opt. Lett. **46**, 5000 (2021).